AIAA JOURNAL
Vol. 44, No. 1, January 2006

Magnetohydrodynamic Power Generation Using Externally Ionized, Cold, Supersonic Air as Working Fluid

Robert C. Murray,* Sohail H. Zaidi,† Mario R. Carraro,‡ Leonid M. Vasilyak,§
Sergey O. Macheret,¶ Mikhail N. Shneider,** and Richard B. Miles††
Princeton University, Princeton, New Jersey 08540

Magnetohydrodynamic (MHD) power extraction from cold air has been demonstrated using short-duration, high-repetition rate, high-voltage pulses (2 ns, 100 kHz, 5 kV/cm) to ionize a Mach 3 (600 m/s), 0.04 kg/m^3 flow. Because the power used to ionize the flow using such a method was less than 1% of the total flow enthalpy, the flow was not heated significantly. A few tens of milliwatts were extracted from the 3-cm cube region of ionization, which scales to hundreds of kilowatts of power in higher velocity, larger-scale devices that would be appropriate for flight applications. Peak electron number densities between 5×10^{11} and 10^{12} cm^{-3} are reported from complementary measurements using microwave absorption in a variable magnetic field. The Hall parameter was estimated from the electrical properties of the MHD channel. Modeling predictions were found to be in agreement with experimentally extracted Faraday current measured between the high-voltage pulses. Modeling also confirmed that the electrons have low energy between the pulses and that the resultant cathode and anode voltage falls are quite low, on the order of 1 V.

Introduction

IN hypersonic flight, high temperatures, short flow times, and strong shock waves pose significant challenges to the structural design, control, and propulsion of vehicles.[1] Because of its ability to generate body forces in a high-speed flow, magnetohydrodynamics (MHD) can provide an innovative way to mitigate some of these challenges.[2,3] MHD forces might, for example, be used for inlet flow control.[3] With MHD body-force interactions, shock waves are not needed to decelerate a hypersonic flow. In addition, MHD generators might be able to extract significant levels of power from the flow[4] to enable new high-power demand technologies including plasma steering, plasma drag reduction, combustion ignition, flame control, and suppression of shock induced separation, all without the need for moving parts.

The viability of MHD flow control and power extraction is expected to improve with increasing altitude and velocity. The need to ionize a flow to make it conductive is perhaps the most significant challenge associated with MHD devices operating in Mach-number regimes below about Mach 12 (Refs. 2–4). In this regime, even the viscous portions of the flow are cold enough such that seeding the flow with an alkali metal vapor will not lead to significant conductivity.[2–4] It has been shown that nonequilibrium ionization methods including electron beams or short, high-voltage pulses are the most efficient means of generating conductivity through ionization.[2–6] It has also been shown that by using nonequilibrium ionization for MHD power extraction the amount of power that can be coupled out of a hypersonic flow can be significantly higher than the theoretical power requirements of ionization.[2–4]

Because of the large density gradients and resultant conductivity gradients associated with supersonic flows, volume-filling supersonic discharges are often difficult to produce in a wind tunnel. In addition to MHD flow control and power generation, there are other applications that render such a discharge desirable. Carbon monoxide and excimer gas discharge lasers in general can benefit greatly from the use of a high throughput of cryogenic gas. To this end, supersonic discharges for pumping such lasers have been reported in molecular flows using dc discharges,[7–9] electron beam stabilization techniques,[10] and a 13.56-MHz rf discharge.[11] Recent progress has been made at the Ohio State University also using a 13.56-MHz rf source to drive a volume-filling discharge in a Mach 2.5 airflow.[12] Pulsed ionization schemes in conjunction with dc discharges have also been implemented successfully in subsonic flows to reduce arcing in CO_2 lasers. This has been demonstrated experimentally by Generalov et al.[13–15]

In the present study, based on Refs. 5 and 6, we use very short (2-ns) pulses with very high the ratio of the electric field strength to the gas number density (E/N) to generate runaway or near-runaway electrons during the pulse.[5,6] We expect the high repetition rate, high-voltage pulse ionization scheme presented here to be several orders of magnitude more efficient than dc or steady rf discharges for generating conductivity and to be more efficient compared with the moderate E/N repetitive-pulse ionization in Refs. 13–15 (Refs. 5 and 6).

Collisions, and their effect on the electrical conductivity, strongly influence the nature of MHD interaction with the flow. The two most relevant parameters in assessing the effects of collisions in a nonthermally ionized MHD generator are the electron Hall parameter Ω_e and the electron loss rate. The Hall parameter is defined as the ratio of the electron-cyclotron frequency eB/m to the electron collision frequency ν_e (Ref. 16). The electron loss rate is dominated at low temperature and high density by attachment to oxygen and at higher ionization levels and lower densities, by electron-ion dissociative recombination.[2–5] Nonuniform flow and nonuniform conductivities, cases where electrons are not the chief current carriers and cases where the magnetic field generated by the MHD current is significant, will add further complications and are neglected in the following discussion.

Presented as Paper 2004-1025 at the AIAA 42nd Aerospace Sciences Meeting, Reno, NV, January 2004; received 16 June 2004; revision received 7 February 2005; accepted for publication 11 February 2005. Copyright © 2005 by the American Institute of Aeronautics and Astronautics, Inc. All rights reserved. Copies of this paper may be made for personal or internal use, on condition that the copier pay the $10.00 per-copy fee to the Copyright Clearance Center, Inc., 222 Rosewood Drive, Danvers, MA 01923; include the code 0001-1452/06 $10.00 in correspondence with the CCC.

*Graduate Student, Department of Mechanical and Aerospace Engineering.
†Research Staff, Department of Mechanical and Aerospace Engineering. Member AIAA.
‡Visiting Ph.D. Student, Department of Mechanical and Aerospace Engineering.
§Research Staff, Department of Mechanical and Aerospace Engineering; currently Director of Research, Institute of High Temperatures, Russian Academy of Sciences, Moscow, Russia.
¶Senior Research Scientist, Department of Mechanical and Aerospace Engineering. Associate Fellow AIAA.
**Research Scientist, Department of Mechanical and Aerospace Engineering. Senior Member AIAA.
††Professor, Department of Mechanical and Aerospace Engineering. Fellow AIAA.

Ionization

Although MHD power extraction onboard a hypersonic vehicle can offer high levels of power generation for use by advanced payloads or engine bypass architectures,[2–4] the power necessary to maintain ionization (and conductivity) is of critical importance to any realistic vehicle. The power required to maintain a given electron number density is a function of two quantities: the energy cost per electron and the rate of electron loss. There are several parameters of interest in hypersonic flow that scale favorably for nonequilibrium ionization in MHD applications, including the following:

1) Low-density flow decreases the power required to sustain a given conductivity because the conductivity is proportional to the ratio of electron and neutral number densities, while the recombination-controlled ionization power budget scales as the square of electron density. Additionally, electron attachment is suppressed at low gas densities.

2) High-velocity flow provides attractive scaling of MHD effects primarily by increasing the voltages and currents associated with an MHD generator. Interestingly, because the flow time through an MHD channel is typically much greater than the lifetime of a free electron in the flow, the increased mass flow rate associated with increasing velocity will, in most cases, incur no penalty with regard to the power requirements necessary to maintain a set volume of ionized flow (in contrast to seeding methods).

3) The unavoidable high temperatures associated with any hypersonic vehicle can often be used as a source of ionization, or to reduce the cost of ionization by suppressing loss processes such as electron attachment to oxygen.

Because thermal ionization at the static temperatures associated with Mach < 12 flow that has passed through a series of oblique shocks is not possible, nonequilibrium ionization methods must be employed.[2–4] From a practical point of view, these nonequilibrium methods of ionization must be able to generate and sustain the ionization with low power input. The power budget for sustaining a nonequilibrium plasma with a prescribed number density is proportional to the energy cost of creating a new electron in the plasma divided by the electron lifetime. When a nonequilibrium plasma is sustained by a dc or oscillating electric field, the electron energy balance is determined by the rate of new electrons generated by other electrons that have been accelerated in the field. The number of those accelerated electrons that have enough energy to overcome the ionization threshold is limited by energy losses in inelastic and elastic collisions with neutral molecules.[17] If the gas density is high, the relevant acceleration time is the time between collisions divided by the mean fraction of electron energy lost per collision. If the gas density is low, the relevant acceleration time is the oscillation cycle of the driving field. Thus the electron temperature, for a given set of gas parameters, is defined by the ratio of electric field strength to the gas number density (E/N), or at low densities, by the ratio of electric field strength to the field oscillation frequency (E/ω).[17] Typical values of E/N in nonequilibrium discharges in molecular gases lie in the range $(1–6) \times 10^{-16}$ V cm (Refs. 2 and 17). The corresponding electron temperatures defined by the electron distribution function's (typically non-Maxwellian) slope at low energy are in the range 1–3 eV (Ref. 17). Under these conditions, only a small fraction of the plasma electrons is capable of ionization that requires 10–15-eV energy. Put simply, the vast majority of electron-molecule collisions result in electron energy loss, but produce no ionization. Therefore, only a very small fraction of the power (less than 0.1%) is actually spent on ionization, and the corresponding energy cost reaches several tens of kiloelectronvolts per electron.[2–5,17]

To achieve higher ionization efficiency, it is desirable to have electrons of very high energy, many times the ionization potential. In this regard high-energy electron beams are a natural choice. Injection of electrons accelerated to kiloelectronvolt and higher energies into a gas results in ionization cascades as the beam propagates and loses its energy. The resulting energy cost per electron is around 34 eV for air, which is only a few times greater than the ionization energy of air molecules.[2–5,18] Models for analyzing plasmas generated by high-energy electron beams have already been applied to supersonic MHD power generation and flow controls.[2–4] Although electron beams are the most efficient way of creating nonequilibrium plasmas, some inherent practical difficulties cannot be ignored. Problems related to mechanical and thermal strengths of injection foils are the main concern, and beam scattering in high-density gases can pose significant constraints on gas penetration.

Problems related to electron-beam-based ionization have provided motivation for the development of alternative techniques for producing high-energy electrons. The most promising of these, for volume-filling plasmas, is through the use of high-voltage pulses.[5,19] In this case high-energy electrons can be produced in situ by applying an electric field that is strong enough to accelerate electrons to above the ionization energy between collisions. To avoid producing an excessive number of electrons and arc formation, the strong electric field is applied for only a very short time. Well before the plasma completely decays, another pulse is applied to generate new electrons. In this way an oscillating electron density with a desired average electron number density can be sustained by matching the pulse repetition rate with the rate of electron loss through recombination or attachment. Modeling predicts that very short, high-voltage pulses at very high repetition rates can sustain a prescribed average ionization level in air with power input a few orders of magnitude lower than would be required for a discharge driven by a conventional dc or oscillating field.[5,6,18,19]

In the current experimental work, a source of multikilovolt, nanosecond pulses with high repetition rate ($\sim$15 kV, 2 ns, 100 kHz) was used to ionize the flow through a Mach 3, continuous electrode Faraday MHD channel. Current/voltage characteristics of the channel are presented. Details on the experimental hardware, theory, and results are included in the following sections.

Experimental Setup

The experiments were conducted in a small-scale, in-draft wind-tunnel facility. The tunnel was configured such that a window viewed directly upstream into the test section. By using this window, the location of the plasma could then be monitored, and, through an iterative process, the pulser electrodes were sized to ensure that the discharge passed through the core of the flow and not through the boundary layer.

Magnet

The magnet used was an Oxford Instruments NiTi, split pair system with three optical axes (bores). A maximum field of 6.5 T is attainable with the system. The field is designed to be uniform over a $3 \times 3 \times 3$ in. ($7.6 \times 7.6 \times 7.6$ cm) cube at the center of the three bores, which are 3×3.5 in. (7.6×8.9 cm) in the spanwise direction (along the horizontal magnetic field lines), 3×3 in. in the streamwise (horizontal) direction, and a 2-in. (5.1-cm)-diam bore in the vertical ($\boldsymbol{u} \times \boldsymbol{B}$) direction.

High-Voltage Pulser

The nonequilibrium plasma was sustained via a custom-made, high-repetition-rate, high-voltage, short-pulse-duration, electrical pulser, model number FPG-30-100, imported from FID Technologies in Russia by Moose Hill Enterprises.[‡‡] The device uses inductors, capacitors, and resistors, along with the switching characteristics of a proprietary diode to create 2-ns, high-voltage, 25-Ω pulses at a maximum repetition rate of 100 kHz. Using a 3×75 Ω cable transformer with an effective output impedance of 225 Ω, the pulser is then capable of generating pulse voltages up to approximately 20 kV, depending on the load impedance.

Mach 3 Flow

Mach 3 laminar flow was achieved through a converging/diverging nozzle. The test cross section measured 1.2×2 in. Because of its optical clarity, resistance to abrasion, electrical insulation, and adequate mechanical properties at elevated temperatures, polycarbonate was used for the tunnel construction.

The tunnel was run in an in-draft setup using an air ejector pump to maintain the low backpressure. The plenum pressure was throttled

[‡‡]Data available online at www.moose-hill.com.

down to 450 torr resulting in laminar flow through the test section with static conditions of 10 torr and 106 K at flow velocity of 620 m/s.

Electrode Setup

All electrodes were machined from aluminum jig plate, in part because jig plate is dimensionally stable for machining shapes with high aspect ratios, and also because aluminum has the lowest cathode voltage drop of any common structural material in air.[17] (The latter property was found to be inconsequential in subsequent studies; see the discussion of experimental and computational results that follows.) A schematic of the pulser electrodes, through which the plasma was sustained, is shown in Fig. 1a.

In preliminary experiments, sharp corners on the pulser electrodes were found to create sufficient heat to erode the polycarbonate tunnel walls. For this reason, the corners of the pulser electrodes were rounded. The electrode geometry was arrived at through an iterative approach. A large plasma volume is desired, but because of the large density gradients (and associated conductivity gradients) across a supersonic flow wider electrodes allow the discharge current to flow mostly through the boundary layer, bypassing the supersonic flow. In the streamwise direction, the plasma needed only to be as long as the power extraction/addition electrodes. Any unnecessarily increased length in this direction needlessly heats the flow and increases the power load on the pulser.

Furthermore, because of the expected high Hall parameter in the flow, spanwise conductivity between the pulser electrodes is expected to be far greater than transverse conductivity. The pulser electrodes are then in relatively good electrical contact with the freestream flow. To minimize their tendency to short out any induced transverse electric field in the $\boldsymbol{u} \times \boldsymbol{B}$ direction, the pulser electrodes were coated with insulating Kapton tape, thus capacitively coupling the pulser to the flow and allowing transverse dc fields to persist. The dimensions of the pulser electrodes are shown in Fig. 1a. Their location in the test section is shown in Figs. 2 and 3.

The design of the MHD power extraction electrodes, which will henceforth be referred to as the MHD electrodes, is subject to three principal constraints:

1) The MHD electrodes must be in contact with the conductive plasma. Because the discharge is in the core flow, these electrodes must extend from the tunnel walls into the discharge.

2) The MHD electrodes must not short out the pulser sustained discharge. Their spanwise width must be small relative to the tunnel width; otherwise, the pulser sustained discharge would be diverted from the supersonic flow into the MHD electrodes, leaving a void in conductivity between the electrodes.

3) The impact of the MHD electrodes on the flowfield should be minimal. Along with condition 2, this suggests a low profile wing geometry.

The resultant MHD electrode design is shown in Fig. 1b. Their location in the test section is shown in Figs. 2 and 3.

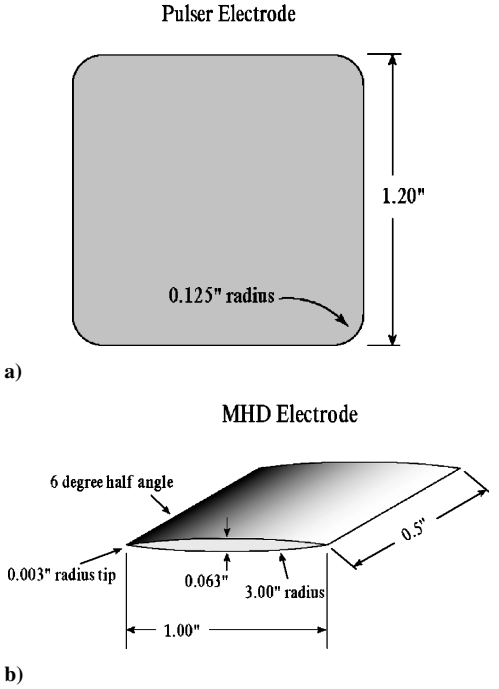

Fig. 1 Schematic of MHD electrodes for a) power addition/extraction and b) pulser electrodes for sustaining conductivity.

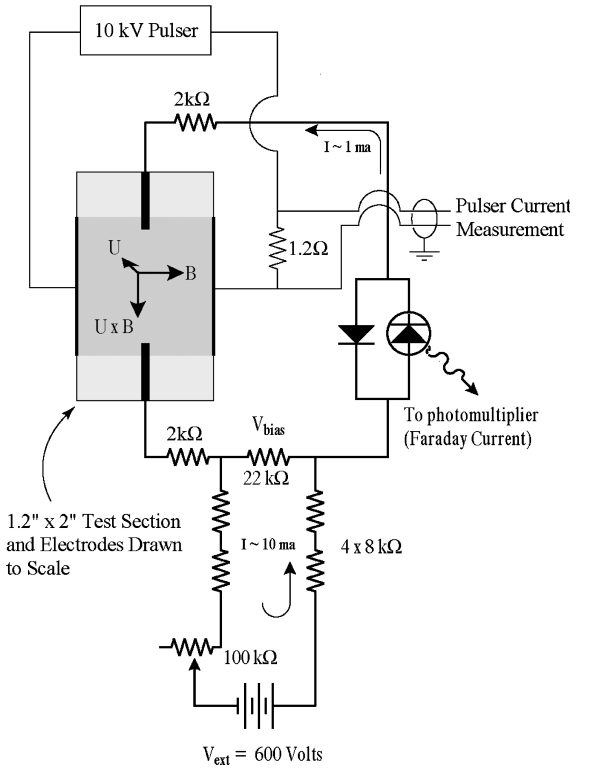

Fig. 2 Diagram of discharge current and Faraday current measurement setup.

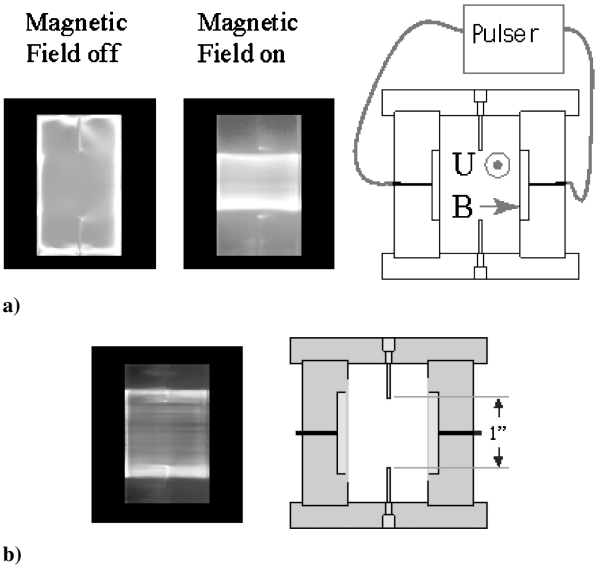

Fig. 3 Images of the operating MHD channel are shown to the left. On the right are scaled sketches of the MHD channel cross section. The camera is downstream, looking upstream at the 1.2 × 2 in. test section. Reflections from the sidewalls have been masked out: a) an earlier setup showing the dramatic effect of the 5-T magnetic field and b) the current setup with the volume filling plasma extending across the cold supersonic freestream and in contact with the MHD electrodes. In this case the pulser electrodes were also insulated with a layer of Kapton tape.

MHD Current Measurement Setup

Electrical noise from the pulser, combined with the interaction of the pulser electrodes and the MHD electrodes, as coupled through the discharge, pose difficult challenges in measuring the Faraday current. For an ideally balanced pulser discharge, the pulser anode and cathode would receive equal and opposite positive and negative voltages respectively. Unfortunately, this is not observed. Because of mainly asymmetric capacitive coupling of the pulser electrodes and their various connecting lines to ground, the MHD electrodes float up and down many kilovolts during a 2-ns pulse. Because of the great disparity in this voltage swing relative to the expected MHD voltage/current characteristics, filtering is not feasible. The solution is to isolate the MHD electrodes (and associated measurement circuit) from ground and to minimize the capacitance of the circuit relative to both ground and free space and to maximize its impedance to the short, high-voltage pulse. A small circuit was constructed using a light-emitting diode (LED) to measure Faraday current in one direction and to achieve optical isolation. A second diode was added to protect the LED from reverse voltages. A resistive bridge was used to provide a bias voltage across the channel with the original intent of overcoming the cathode sheath voltage. The resistance bridge also provides isolation between the MHD electrodes and the laboratory.

The device was calibrated by connecting a function generator in parallel with the MHD electrodes. Current was determined by measuring the voltage across one of the 2-kΩ resistors with an oscilloscope. This was compared with the output of the photomultiplier tube (PMT), also measured on an oscilloscope. The LED/PMT circuit was found to have a threshold of 75 μA, a sensitivity of 20 mV/mA, and, aside from propagation delay, a frequency response in excess of 100 MHz.

Discharge Current Measurement Setup

The discharge current through the pulser electrodes was measured by placing a 1.2-Ω shunt (consisting of ten 12 Ω low-inductance, carbon resistors) in series with the pulser as shown in Fig. 2. This setup measures both displacement and conductive current through the channel.

Imaging

A Fuji 2800 charge-coupled-device (CCD) camera was used to record images of the discharge in the MHD channel. CCD cameras have been found to be resistant to magnetic fields on the order of 1 T and to electrical noise generated by the pulser. The camera has a $6\times$ optical zoom, allowing it to be placed at a safe distance from the magnet. The camera was positioned downstream of the test section and looked directly upstream at the discharge through an acrylic window.

Relevant Parameters

In complementary investigations of air in a static cell at similar densities, the, electron collision frequency has been found to be on the order of 5–10 GHz, and not a strong function of neutral gas density.[20] The resultant electron Hall parameter is then $\Omega_e > 90$. This has several repercussions that will be addressed in detail in the modeling section at the end of this paper. An immediate consequence of the extremely high Hall parameter for the experiments is that the conductivity in the spanwise direction $\sigma_\parallel$ is expected to be far greater than the conductivity in the transverse direction $\sigma_\perp$. We would then expect a huge disparity when comparing conductivities between the MHD electrodes to conductivities between the pulser electrodes. The magnetic field is therefore expected to have a dramatic effect on the current path of the discharge. A benefit of the relatively high spanwise conductivity is to increase the effective area of the MHD electrodes by allowing them to draw Faraday current from a wider area of the plasma than their cross section would suggest. A drawback of the relatively high spanwise conductivity is that it tends to put the sidewall boundary layers in parallel electrical contact with the core freestream, effectively reducing the emf we would expect to see.

Because the peak currents delivered by the pulser are expected to far exceed the normal cathode current density, we expect electron emission from the entire cathode. Ideally, the effect of the magnetic field would be to maintain this current "footprint" across the discharge to the anode, resulting in a uniform, volume-filling discharge.

The total flow enthalpy entering the test section is 12 kW. The total power available from the pulser is approximately 100 W. Even with perfect impedance matching, the pulser is not able to significantly heat the bulk flowfield. The working fluid in the MHD channel will then be cold air.

The flow time through the MHD channel, which is taken to be the time it takes for the freestream flow to convect over the pulser electrodes, is about 42 μs. This corresponds to about four of the 100-kHz high-voltage pulses.

Budgetary and time constraints necessitate a relatively small-scale experimental facility. This will tend to reduce MHD effects for three reasons:

1) Sheath voltages will tend to remain constant with respect to the length scale of an MHD channel. Conversely, the voltage scale of an MHD generator (uBd) will increase linearly with length scale. In this experiment uBd is 600 m/s $\times$ 5 T $\times$ 3 cm $=$ 90 V, which is smaller than the cathode voltage drop of 230 V for an aluminum cathode in air.[17] Whereas in a large-scale facility this voltage drop would be small or negligible with respect to the emf across the channel, it is a dominant feature in this experiment.

2) Although we expect a significant Hall parameter, the relatively short length of our interaction region (about 1 in.) reduces the aspect ratio of the channel, which, in turn, makes electrode segmentation and Hall-generator setups difficult. In addition, the fraction of energy removed from a given flow increases with the length of the channel, regardless of aspect ratio. A full-scale MHD generator would likely be considerably longer than one inch.

3) In low-Reynolds-number wind-tunnel flows the boundary layer comprises a relatively large fraction of the flowfield. Dealing with large boundary layers and their associated conductivity gradients complicates the design of an MHD channel.

Results and Discussion

Images of Discharge

Images of the discharge are shown in Fig. 3 along with a scaled sketch of the MHD channel cross section. The images were taken from downstream of the MHD channel looking upstream towards the test section. Whereas row b in Fig. 3 corresponds to the present setup, row a is presented to show the dramatic effect of magnetic field on the discharge. Without the applied magnetic field, the lower-density boundary layer presents the easiest current path between the electrodes. As expected, the 5-T magnetic field has a dramatic effect on the conductivity of the flowfield and appears to maintain the current footprint of the cathode across the discharge.

A scale diagram of the present channel is shown in Fig. 3b. In this case the pulser electrodes were widened so as to ionize a greater fraction of the flow (60% of the flow passes through the discharge). The tips of the MHD electrodes are in contact with the plasma, and there is a clear conductive path through the high-velocity core flow. The additional step of covering the pulser electrodes with Kapton tape was implemented to ensure that the Faraday current would not be shorted out through the pulser electrodes. The uninsulated pulser electrodes were found to neutralize all vertical (transverse) electric fields in the discharge to below measurable levels.

Horizontal layers of varying brightness are seen in all instances of the discharge with the magnetic field on. These are believed to be caused by nonuniformities in emission from the cathode and are currently a subject of investigation.

Pulse Current and Voltage

The resistive shunt used to measure the discharge current supplied by the pulser is shown in Fig. 2. To determine the approximate impedance of the plasma, resistors were placed in series with the pulser electrodes with one standard atmosphere of air in the wind-tunnel test section (sufficient to prevent breakdown). Time traces of the resulting voltages were recorded on an oscilloscope. Oscilloscope traces corresponding to several resistor values were compared to traces corresponding to breakdown through the Mach 3 flow. Visual analysis of shunt signals showed that after breakdown

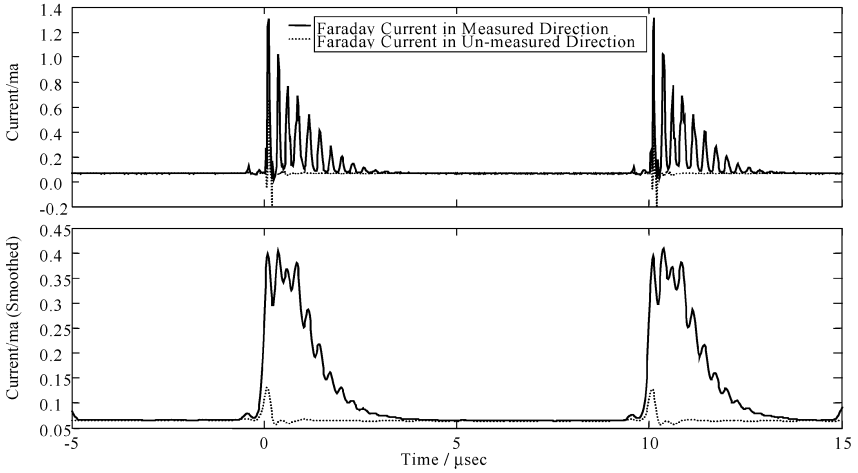

Fig. 4 Faraday current measurements with the magnetic field in each direction. Ringing in the top plot is due to an interaction with the bias circuit. In the bottom graph, the plot has been smoothed with a 250-ns Gaussian window.

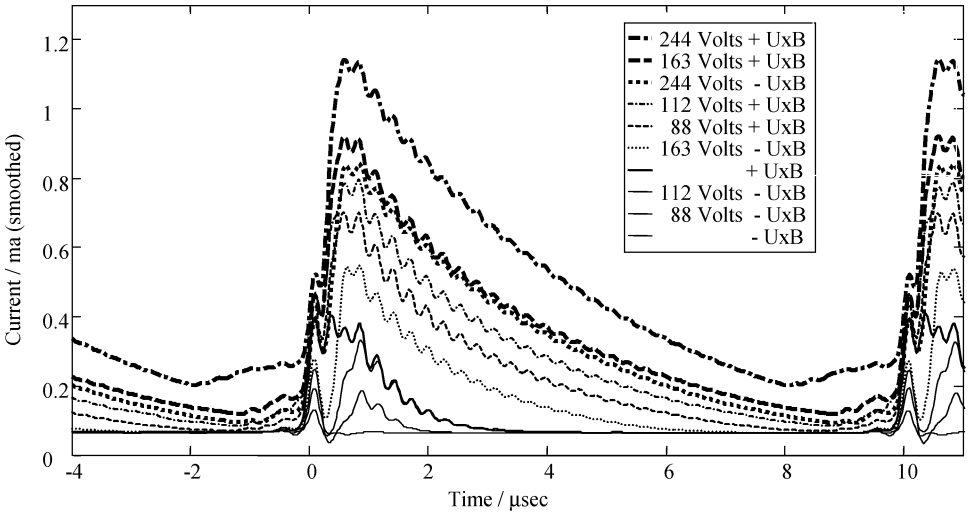

Fig. 5 Faraday current measurements with different bias voltages and magnetic field directions (smoothed with a 250-ns Gaussian window). For clarity, the order of the curves from top to bottom is the same as the order in the legend. The sign of the $U \times B$ voltage pertains to the direction in which current can be measured.

the resistance of the discharge was approximately 1 kΩ (relative to the pulser).

For an ideal cable transformer, effectively carrying a 225-Ω 10-kV pulse, we would expect the voltage peak at the pulser electrodes to be nearly 20 kV. However, capacitive coupling among the electrodes, their connections to the cable transformer, the magnet body, and free space all tend to reduce the impedance of the load on the pulser. The actual voltage across the pulser electrodes is estimated to peak at approximately 15 kV. This corresponds to a discharge current on the order of 15 amps through the equivalent 1-kΩ resistance.

Faraday Current and Voltage

The principle employed to measure Faraday current was as follows. The MHD channel was run with the magnetic field set to 5 T. Using the circuit shown in Fig. 2, the PMT voltage trace corresponding to Faraday current was recorded on an oscilloscope. Because the circuit is only sensitive to current in one direction, the magnetic field direction was then reversed, and data were recorded a second time. It was assumed that the pulser driven discharge and associated electrical noise would be unaffected by a magnetic field reversal. Switching the magnetic field should then isolate the measurement of the MHD current from the noise associated with the pulser. The resultant current traces shown in Fig. 4 do show a clear difference in the transverse currents driven across the flowfield using different magnetic field directions. To our knowledge the traces presented in Fig. 4 represent the first demonstration of MHD current extracted from a cold supersonic flow.

Although the current measurement circuit was calibrated to measure current to within less than 5% of the actual value, the 2-MHz ringing seen in Fig. 4 is caused by the connection of the external batteries (via 3 m of twisted pair wire necessary to physically remove the batteries from the intense magnetic field) shown in Fig. 2. The ringing was not observed before the bias voltage portion of the circuit was connected. This appears to limit the response frequency of the current measurement circuit to about 2 MHz, which is presumed to be the most significant uncertainty in the data. To make the data easier to interpret visually, it was smoothed using a 250-ns (half-width) Gaussian function.

To gain further insight into the electrical characteristics of the MHD channel, current measurements were recorded using a variety of externally applied bias voltages and are presented in Fig. 5. In all cases the current traces are periodic at the pulse rate of 100 kHz. As in Fig. 4, these current traces are smoothed with a 250-ns Gaussian window. Also, in the unbiased cases no Faraday current was recorded until the pulser electrodes were insulated with Kapton foil. The nude pulser electrodes were apparently able to neutralize the induced transverse electric fields. The Kapton foil did not cause any noticeable change in the pulser-driven discharge.

Information as to the Thevenin's equivalent Faraday voltage can be gleaned from the data presented in Fig. 5. The cases corresponding to 112 V $-\boldsymbol{u}\times\boldsymbol{B}$ and $+\boldsymbol{u}\times\boldsymbol{B}$ are very similar. This implies the Faraday voltage to be 56 V. The fact that current is measured in the 88 V $-\boldsymbol{u}\times\boldsymbol{B}$ case suggests the Faraday voltage is less than 88 V, which is consistent with the 56-V estimate.

If the Faraday voltage is assumed to be 56 V, and considering that the peak currents in Fig. 5 range from 0.4 to 1.1 mA for corresponding voltages ranging from 56 to 300 V, then peak conductivities across the MHD generator correspond to resistance levels of 140 to 270 kΩ, which, neglecting geometrical effects, suggests the spanwise/transverse conductivity ratio ($\sigma_\perp/\sigma_\parallel$) to be about 200; the Hall parameter is high.

Also, even with voltages far lower than the normal cathode fall, self-sustained currents are in fact being driven across the flow. At an electron number density of $\sim 10^{11}$ cm^{-3} over the plasma volume,[10] the total Faraday current could be maintained by extracting less than 1% of the total charge created by the pulsed discharge. At the high Hall parameters in our experiments, electron currents are suppressed, and ion currents are significant. (See the modeling results in the next section.) The comparable contribution of ions and electrons to the total current essentially eliminates the basic reason for a significant cathode voltage fall.

Scaling

As mentioned earlier, this experimental setup is considerably smaller and slower than the intended flight-scale application.[2–4] With a relatively low enthalpy extraction ratio, the effects on the flow would not be strong, and the total cost of ionization required to sustain the same conductivity and the total extracted power would be expected to scale linearly with the volume of a larger MHD channel. The extracted power also scales as the velocity squared. Whereas our experiment had an approximately $3\times3\times3$ cm MHD region and a 600-m/s flow, a flight scale device could have a volume on the order of 10 m^3 at three times the velocity. This would scale up to roughly 10 million times the power levels reported here, or hundreds of kilowatts, as opposed to tens of milliwatts.

Modeling of Dynamics of Decaying Plasma in MHD Section

To understand plasma kinetics and dynamics between the pulses and to infer the peak electron density from the experiments, we conducted modeling. In the modeling, the flow was in the x direction, the B field in the z direction, and the Faraday current in the y direction. The modeling was quasi one dimensional in the y direction. All calculations were performed for the experimental conditions: $p=10$ torr, $T=106$ K, $u=620$ m/s, and $B=5$ T. The spacing between the MHD electrodes was 3 cm.

To analyze the dynamics of decaying plasmas in the cold air MHD channel, we used the following set of continuity equations for plasma electrons (number density n_e) and positive (n_+) and negative (n_-) ions, plus the Poisson equation (4) for the electric potential[6,17]:

$$\frac{\partial n_e}{\partial t}+\frac{\partial \Gamma_e}{\partial y}=k_d N n_- - \nu_a n_e - \beta n_e n_+ \tag{1}$$

$$\frac{\partial n_+}{\partial t}+\frac{\partial \Gamma_+}{\partial y}=\beta_{ii} n_- n_+ - \beta n_e n_+ \tag{2}$$

$$\frac{\partial n_-}{\partial t}+\frac{\partial \Gamma_-}{\partial y}=-k_d N n_- + \nu_a n_e - \beta_{ii} n_- n_+ \tag{3}$$

$$\frac{\partial^2 \varphi}{\partial y^2}=-\frac{e}{\varepsilon_0}(n_+-n_e-n_-), \qquad E_c=-\frac{\partial\varphi}{\partial y} \tag{4}$$

Here Γ_e, Γ_+, and Γ_- are the fluxes of charged particles, N is the neutral molecule number density, β, β_{ii} are the electron-ion and ion-ion recombination rate coefficients, ν_a is the attachment frequency, k_d is the detachment rate coefficient, φ is the electric potential, and E_C is the electric field produced by the space charge in the sheath regions and by surface charges on the electrodes.

Taking into account ion slip[16] and assuming that positive and negative ions have identical transport properties, the fluxes of charged species can be written in the drift approximation as

$$\Gamma_e=\begin{cases}-\dfrac{\mu_e n_e E}{(1+\Omega_e\Omega_+)(1+\tilde{\Omega}_e^2)}, & \text{continuous electrodes}\\[2ex] -\dfrac{\mu_e n_e E}{(1+\Omega_e\Omega_+)}, & \text{segmented electrodes}\end{cases} \tag{5a}$$

$$\Gamma_\pm=\pm\mu_+ n_{+,-} E/(1+\Omega_+\Omega_-) \tag{5b}$$

Here $\mu_{e,\pm}$ are the mobilities of electrons and positive and negative ions at $B=0$; and electron, ion, and the effective Hall parameters are

$$\Omega_e=eB/m\nu_{en}\equiv\mu_e B$$

$$\Omega_+=eB/M\nu_{in}\equiv\mu_+ B$$

$$\tilde{\Omega}_e=\Omega_e/(1+\Omega_e\Omega_+)$$

The electric field E in the MHD generator channel to be used in expressions (5) for the fluxes is

$$E=uB+E_c \tag{6}$$

For fluxes of charged species, we used standard boundary conditions at the electrodes. These conditions are commonly used to model gas discharges with cold cathodes[17]: at $y=0$ (MHD cathode),

$$\Gamma_e=-\gamma\Gamma_+, \qquad \Gamma_-=0 \tag{7}$$

and, at $y=L_y$ (MHD anode),

$$\Gamma_+=0, \qquad \left.\frac{\partial\Gamma_{e,-}}{\partial y}\right|_{y=L_y}=0 \tag{8}$$

where γ is the effective secondary emission coefficient, that is, the average number of electrons emitted for each ion impinging on the surface. In our conditions, the results are only weakly sensitive to the value of γ. In the present calculations, we set $\gamma=0.1$.

Equations (1–8) were solved using the following approach: The drift approximation of the continuity equations (1–3) for the charge densities are hyperbolic equations. To solve them, we used an explicit, second order in space and first order in time scheme[21] that has previously been successfully used for pulsed discharge[22] and streamer[23] modeling. In each time step the elliptic Poisson equation (4) was solved for the instantaneous distribution of charge densities by the standard tridiagonal matrix Thomas algorithm[24] with second-order accuracy.

Boundary conditions for the Poisson equation (4) are

$$\varphi(0)=0, \qquad \varphi(L_y)=k|uB|L_y \tag{9}$$

where k is the load factor. The value of k is about 0.6 during the pulse, but, as the plasma decays and its resistance increases, the MHD circuit approaches $k=0$ (short circuit). In this work, we did not couple the full equation for the circuit with other equations. Instead, calculations were performed at $k=0$ and 0.6.

In the general case, the Faraday current decays because of both plasma decay and the reduction in electromotive force caused by the field produced by the charge separation in the cathode sheath.

The results of analysis of ionization and ion conversion processes, using the rates compiled in Ref. 25, can be summarized as follows. During the short, 2-ns pulse, electrons acquire high energies and ionize air molecules producing primary ions N_2^+ and O_2^+. At the relatively high density and very low temperature in the test section ($p=10$ torr, $T=109$ K), the ions N_2^+ are also rapidly converted into O_2^+ in two stages:

$$N_2^+ + N_2 + N_2 \rightarrow N_4^+ + N_2 N_4^+ + O_2 \rightarrow O_2^+ + N_2 + N_2$$

O_2^+ ions are rapidly converted into O_4^+ cluster ions via the following processes:

$$O_2^+ + O_2 + O_2 \rightarrow O_4^+ + O_2O_2^+ + N_2 + N_2$$

$$\rightarrow O_2^+ \cdot N_2 + N_2O_2^+ \cdot N_2 + O_2 \rightarrow O_4^+ + N_2$$

The entire ion conversion occurs on a submicrosecond timescale and results in O_4^+ being the dominant positive ion. The dissociative recombination with cluster ions $e + O_4^+ \rightarrow O_2 + O_2$ is much faster than the dissociative recombination with simple molecular ions, and, together with the three-body attachment $e + O_2 + O_2 \rightarrow O_2^- + O_2$, it determines the plasma decay after the pulse.

The rate coefficients are[6,17,25]

$$\beta = 1.4 \times 10^{-6} \times (300/T_e)^{1.5}\ \mathrm{cm^3/s} \quad \text{for} \quad O_4^+ + e \rightarrow O_2 + O_2$$

$$\nu_a = k_a N_{O_2}^2$$

$$k_a = 1.4 \times 10^{-29} \times 300/T_e \times \exp(100/T - 700/T_e)\ \mathrm{cm^6/s}$$

$$k_d = 2.7 \times 10^{-10} \times (T/300)^{0.5} \times \exp(-5590/T)\ \mathrm{cm^3/s}$$

$$\beta_{ii} = 2 \times 10^{-25} \times (300/T)^{2.5} \times N\ \mathrm{cm^3/s} \quad \text{if} \quad \rho < \rho_0 \times (T/300)^{1.5}$$

$$\beta_{ii} = 5.374 \times 10^{-6} \times (\rho_0/\rho)\ \mathrm{cm^3/s} \quad \text{if} \quad \rho \geq \rho_0 \times (T/300)^{1.5}$$

(where ρ_0 is the atmospheric density at standard temperature and pressure).

The electron mobility $\mu_e = e/m\nu_{en}$, and, therefore, electron Hall parameter Ω_e, strongly depend on electron temperature. We used the values

$$\mu_e(T_e)N = v_d(E_{\mathrm{eff}}/N)/(E_{\mathrm{eff}}/N), \qquad T_e = T_e(E_{\mathrm{eff}}/N)$$

determined from the experimental values tabulated in Ref. 26, $v_d(E/N)$ and $T_e(E/N)$, where v_d is the drift velocity.

The electron temperature in the plasma corresponds to the instantaneous effective electric field value:

$$\frac{E_{\mathrm{eff}}}{N} = \begin{cases} \dfrac{E}{N(1+\Omega_e\Omega_+)\sqrt{1+\tilde{\Omega}_e^2}}, & \text{continuous electrodes} \\ \dfrac{E}{N(1+\Omega_e\Omega_+)}, & \text{segmented electrodes} \end{cases} \tag{10}$$

The results of modeling in the assumption of Faraday generator with continuous electrodes are shown in Figs. 6–11. Perhaps the most surprising result is shown in Fig. 7: the cathode voltage fall does not exceed a few volts. This is explained by the following. Because of the high value of Hall parameter, the Faraday current and the effective electric field are weak. Because of the weak electric field, the electron temperature in the decaying plasma is very low, as seen in Fig. 6. The collision rate of the low-energy electrons is quite low,

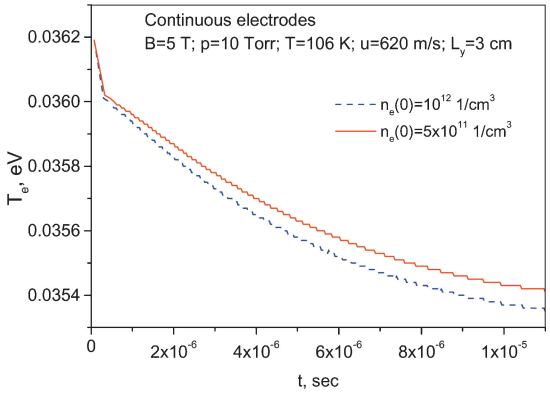

Fig. 6 Electron temperature after the pulse in the Faraday generator with continuous electrodes.

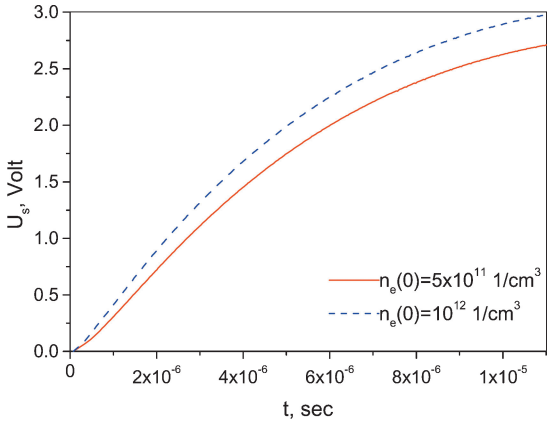

Fig. 7 Cathode sheath voltage fall after the pulse in the Faraday generator with continuous electrodes.

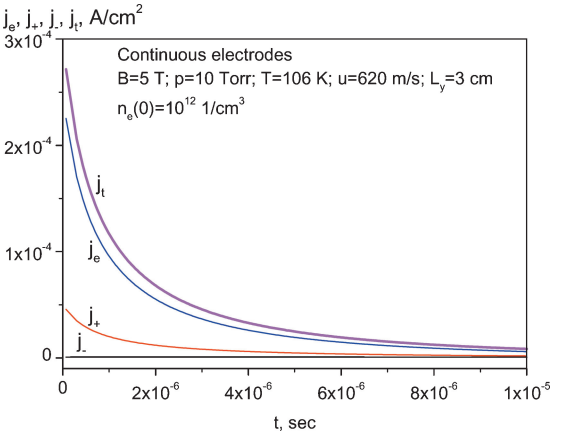

Fig. 8 Current densities in the midplane between the electrodes ($y = L_y/2$): electron current j_e, positive ion current j_+, negative ion current j_-, and the total current $j_t = j_e + j_+ + j_-$, calculated in the assumption $k = 0$, at two different values of initial (peak) electron density in the Faraday generator with continuous electrodes.

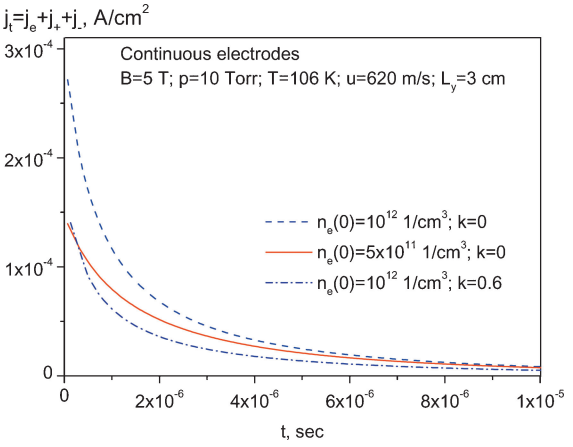

Fig. 9 Total current densities in the middle of the gap ($y = L_y/2$) at different values of k and $n_e(0)$ in the Faraday generator with continuous electrodes.

leading to both high scalar conductivity and high Hall parameter. Therefore, the effective electron conductivity[16] $\sigma_{\mathrm{eff}} = \sigma/(1+\Omega^2)$ is quite low. In fact, as seen in Fig. 8, the electron conductivity becomes so low that the electron current is not much stronger than the ion current. This eliminates the principal reason for a substantial cathode fall (the sharp difference between electron and ion mobilities).

Because the cathode fall is insignificant, the decrease of the current with time after the pulse is caused by the bulk losses of electrons and ions in recombination and attachment. As seen in Fig. 10, both

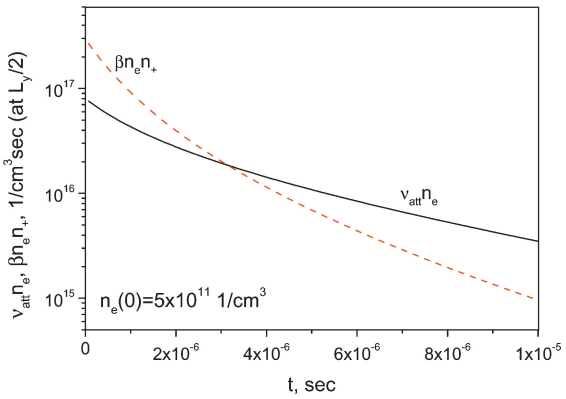

Fig. 10 Comparison of different mechanisms of losses: dissociative recombination and attachment at $n_e(0) = 5 \times 10^{11}$ 1/cm^3 in the Faraday generator with continuous electrodes.

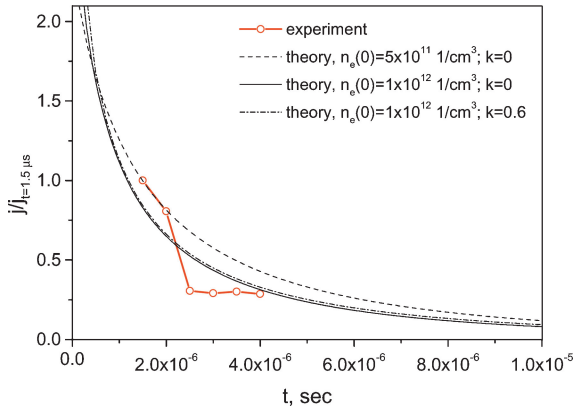

Fig. 11 Comparison of the calculated normalized current density for continuous-electrode Faraday generator with experiment.

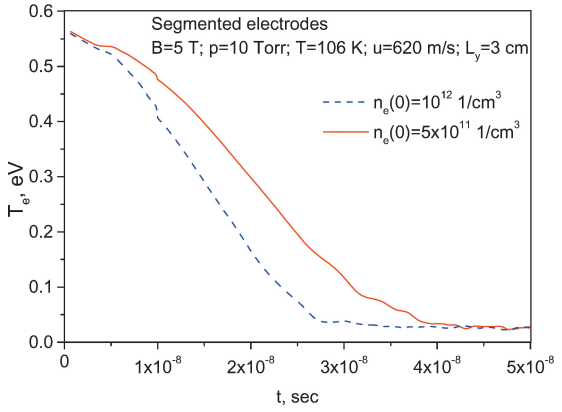

Fig. 12 Electron temperature after the pulse in the ideal Faraday generator with segmented electrodes and $k = 0$.

recombination with cluster ions and three-body attachment to oxygen make a comparable contribution to the experimentally observed decay rate.

As seen in Fig. 11, the computed decay of the current for the initial value of $n_e = 5 \times 10^{11}$–10^{12} cm^{-3} agrees well with the experimental data. The comparison centers around the current measurement in the vicinity of 2 μs after the voltage pulse. Before this time, the measurement circuit has not had time to respond to the Faraday current, and after this time the current falls below the threshold of measurement. The absolute value of the peak current density, 0.15–0.3 mA/cm^2 (see Figs. 8 and 9), together with the estimated effective current-collection area of a few square centimeters, is in good agreement with the experimentally measured peak current.

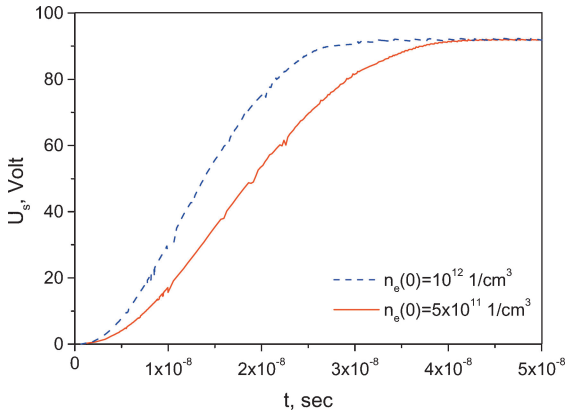

Fig. 13 Cathode voltage fall after the pulse in the ideal Faraday generator with segmented electrodes and $k = 0$.

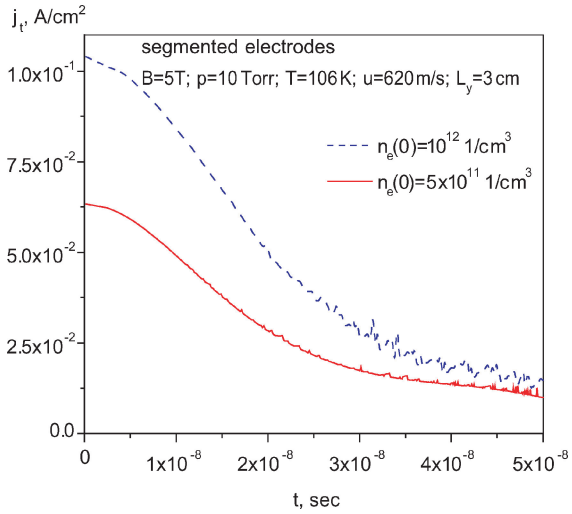

Fig. 14 Total current density in the middle of the gap ($y = L_y/2$) after the pulse in the ideal Faraday generator with segmented electrodes and $k = 0$.

Modeling was also performed for an ideal segmented-electrode Faraday generator. The results, shown in Figs. 12–14, are dramatically different from the continuous-electrode case. The Faraday current is initially strong, and the relatively strong Faraday electric field in the channel heats the electrons (Fig. 12). This results in the rapid (on 10-ns timescale) growth of cathode voltage fall, depicted in Fig. 13. The rapid growth of the cathode sheath leaves very little voltage for the quasineutral plasma, and the current drops very quickly (much faster than in the experiments), even with little recombination and attachment. This should be taken into account when planning experimental work with segmented-electrode MHD devices.

Conclusions

A volume-filling, uniform, nonequilibrium, cold plasma has been produced in a Mach 3 airflow using 2-ns, 100-kHz repetition rate, 30-kV pulses. Theoretical analysis indicates the electron number density to be on the order of 5×10^{11}–10^{12} cm^{-3}.

The 5-T magnetic field was shown to improve the uniformity of the plasma and had a dramatic effect in confining the plasma to the interelectrode volume.

For the first time, an experimental observation of magnetohydrodynamic (MHD) power extraction using nonequilibrium ionization in a cold supersonic airflow has been made.

By varying an applied bias voltage across the MHD channel, the Faraday voltage was measured to be 60% of the theoretical value.

Modeling of the Faraday generator with continuous electrodes revealed that, in the plasma decaying between the pulses, the cathode

voltage fall does not exceed a few volts, the electron current is not much stronger than the ion current, and current decreases due to electron recombination with cluster ions and three-body attachment to oxygen. In contrast, a sharp increase of the cathode voltage fall and cutoff of the current is predicted for segmented-electrode Faraday devices.

Acknowledgments

This work was supported in part by the MARIAH II Wind Tunnel Project with funding from the U.S. Air Force Arnold Engineering Development Center under subcontract from MSE Technology Applications, Inc., and in part by the Air Force Office of Scientific Research under John Schmisseur.

References

[1]Curran, E. T., and Murthy, S. N. B. (eds.), *Scramjet Propulsion*, Vol. 189, Progress in Astronautics and Aeronautics, AIAA, Reston, VA, 2000.

[2]Macheret, S. O., Shneider, M. N., and Miles, R. B., "Electron Beam Generated Plasmas in Hypersonic MHD Channels," *AIAA Journal*, Vol. 39, No. 6, 2001, pp. 1127–1138.

[3]Macheret, S. O., Shneider, M. N., and Miles, R. B., "Magnetohydrodynamic Control of Hypersonic Flows and Scramjet Inlets Using Electron Beam Ionization," *AIAA Journal*, Vol. 36, No. 1, 2002, pp. 74–81.

[4]Macheret, S. O., Shneider, M. N., and Miles, R. B., "MHD Power Extraction from Cold Hypersonic Air Flow with External Ionizers," *Journal of Propulsion and Power*, Vol. 18, No. 2, 2002, pp. 424–431.

[5]Macheret, S. O., Shneider, M. N., and Miles, R. B., "Modeling of Air Plasma Generation by Electron Beams and High-Voltage Pulses," AIAA Paper 2000-2569, June 2000.

[6]Macheret, S. O., Shneider, M. N., and Miles, R. B., "Modeling of Air Plasma Generation by Repetitive High-Voltage Nanosecond Pulses," *IEEE Transactions on Plasma Science*, Vol. 30, No. 3, Pt. 2, 2002, pp. 1301–1314.

[7]Vallach, E., Zeevi, A., Greenfield, E., and Yatsiv, S., "Transverse Excitation Pulsed Laser in Gas-Dynamically Cooled Mixtures," *Applied Physics Letters*, Vol. 20, No. 10, 1972, p. 395.

[8]Blom, J. H., Hanson, R. K., "Double-Discharge Arrangement for cw Electrical Excitation of Supersonic Flows," *Applied Physics Letters*, Vol. 26, No. 4, 1975, p. 190.

[9]Jones, T. G., Byron, S. R., Hoffman, A. L., O-Brian, B. B., and Lacuna, W. B., "Electron-Beam-Stabilized CW Electric Discharge Laser in Supersonically Cooled Co/N_2/Ar Mixtures," AIAA Paper 74-562, June 1974.

[10]Forestier, B. M., Fontaine, B. L., and Gross, P., "Dynamics of Supersonic Flow Eximer Lasers," AIAA Paper 80-1432, July 1980.

[11]Uehara, M., and Kanazawa, H., "Experimental Study on Operation at Room Temperature of Transverse Flow Carbon Monoxide Laser Excited by Radio Frequency Discharge," *Applied Physics Letters*, Vol. 65, No. 1, 1994, pp. 22–24.

[12]Palm, P., Meyer, R., Plonjes, E., Rich, W., and Adamovich, I., "Nonequilibrium Radio Frequency Discharge Plasma Effect on Conical Shock Wave: M = 2.5 Flow," *AIAA Journal*, Vol. 41, No. 3, 2003, pp. 465–469.

[13]Generalov, N. A., Zimakov, V. P., Kosynkin, V. D., Raizer, Y. P., and Roitenburg, D. I., "Method for Significantly Increasing the Stability Limit of the Discharge in Fast-Flow Large-Volume Lasers," *Soviet Technical Physics Letters*, Vol. 1, No. 5, 1975, pp. 201, 202.

[14]Generalov, N. A., Zimakov, V. P., Kosynkin, V. D., Raizer, Y. P., and Roitenburg, D. I., "Stationary Non-Self-Sustained Discharge with High-Voltage Electrodeless Ionization in the Closed Cycle Laser," *Soviet Journal of Plasma Physics*, Vol. 3, No. 3, 1977, pp. 526–643 (in Russian).

[15]Generalov, N. A., Zimakov, V. P., Kosynkin, V. D., Raizer, Y. P., and Solov'ev, N. G., "Rapid-Flow Combined-Action Industrial CO_2 Laser," *Soviet Journal Quantum Electronics*, Vol. 12, No. 8, 1992, pp. 993–998.

[16]Rosa, R. J., *Magnetohydrodynamic Energy Conversion*, McGraw–Hill, New York, 1968.

[17]Raizer, Yu. P., *Gas Discharge Physics*, Springer-Verlag, Berlin, 1991, Chaps. 1–8.

[18]Macheret, S. O., Shneider, M. N., and Miles, R. B., "Modeling of Discharges Generated by Electron Beams in Dense Gases: Fountain and Thunderstorm Regimes," *Physics of Plasmas*, Vol. 8, No. 5, 2001, pp. 1518–1528.

[19]Macheret, S. O., Shneider, M. N., and Miles, R. B., "Modeling of Air Plasma Generation by Repetitive High-Voltage Nanosecond Pulses," *IEEE Transactions on Plasma Science*, Vol. 30, No. 3, Pt. 2, 2002, pp. 1301–1314.

[20]Zaidi, S. H., Murray, R. C., Carraro, M., Valilyak, L. M., Shneider, M. N., Macheret, S. O., and Miles, R. B., "Diagnostics of Short-Pulsed, Sustained Plasmas in a Cold Air MHD Channel," AIAA Paper 2004-0708, Jan. 2004.

[21]Roache, P. J., *Computational Fluid Dynamics*, Hermosa, Albuquerque, NM, 1972, Chap. 3.

[22]Raizer, Y. P., and Shneider, M. N., "Electrodeless Capacitive Discharge Sustained by Repetitive High-Voltage Pulses," *High Temperature*, Vol. 27, No. 3, 1989, pp. 327–335.

[23]Kulikovsky, A. A., "The Structure of Streamers in N_2 I: Fast I Method of Space-Charge Dominated I Plasma Simulation," *Journal of Physics D*, Vol. 27, Dec. 1994, pp. 2556–2563.

[24]Anderson, D. A., Tannehill, J. C., and Pletcher, R., *Computational Fluid Mechanics and Heat Transfer*, Hemisphere, New York, 1984, Chap. 4.

[25]Kossyi, A., Kostinsky, A. Y., Matveyev, A. A., and Silakov, V. P., "Kinetic Scheme of the Non-Equilibrium Discharge in Nitrogen–Oxygen Mixtures," *Plasma Sources Science and Technology*, Vol. 1, No. 3, 1992, pp. 207–220.

[26]Grigoriev, I. S., and Meilikhov, E. Z. (eds.), *Handbook of Physical Quantities*, CRC Press, Boca Raton, FL, 1997, Chap. 21.

M. Auweter-Kurtz
Associate Editor